This project has received funding from the European Union's Horizon 2020 research and innovation programme under grant agreement No 871813.

MUNDFAB

ICT Project No 871813

MUNDFAB

Modeling Unconventional Nanoscaled Device FABrication

D4.3: First round of experiments on structural modifications, alloy redistribution to validate model predictions, experimental plan for second round

R. Demoulin (CNRS), R. Daubriac (CNRS), P. Acosta Alba (CEA), S. Kerdiles (CEA), F. Cristiano (CNRS)

26/07/2021

Fraunhofer IISB leti ceatech cnrs Łukasiewicz Instytut Technologii Materiałów Elektronicznych life.augmented TU WIEN

Quality management

This deliverable was reviewed by:

Sylvain Joblot, STMicroelectronics

Pawel Michalowski, Ł-IMiF

Contents

Abstract

This deliverable reports on the first round of experiments for the characterization of the structural evolution induced by laser annealing on undoped and Boron-doped strained SiGe thin layers. The structural characterization has been carried out using numerous experimental processes (SIMS, AFM, TEM, …) which allowed to evidence a significant impact of the laser energy density on the whole SiGe layer. In fact, depending of the laser energy density, four different annealing regimes have been described and each of them can be characterized by (i) a redistribution of the Ge all along the layer thickness, (ii) a modification of the crystalline quality and (iii) a nano-structuration of the layer surface. In the specific case of Boron doping, four-point probe and Hall measurements highlighted that these structural modifications led also to changes of the electrical properties. However, the correlation between structural and electrical properties remains under discussion. Finally, this deliverable also presents the prospects in order to improve the understanding of the structural evolution of SiGe layers induced by laser annealing.

1. Introduction

The results presented in this deliverable are related to the work carried out in task 4.2 of the MUNDFAB project, whose main objective is to develop models for the description of the structural modifications of undoped and doped SiGe nanostructures upon laser annealing. To this purpose, dedicated experiments have been performed within this task to support the model development. Here, the first experimental investigations performed to characterize the evolution of SiGe layers as function of the laser annealing conditions are presented. Multiple studies (using SIMS, ToF-SIMS, TEM, STEM-HAADF, …) have been carried out in order to characterize the Ge segregation and the modifications in the crystalline quality induced by the laser annealing. Moreover, AFM experiments were performed to identify the surface structuration generated by such annealing. Finally, VdP-Hall effect and four-point probe measurements were used to measure the overall activation level in terms of active dose in B-doped SiGe layer.

The characteristics of all analysed samples are briefly summarized in the first part. Then, the structural evolution of the $Si_{1-x}Ge_x$ layer as a function of the laser annealing conditions and depending on the layer parameters are described. A strong interest has been focused on the Ge diffusion and the strain state of the $Si_{1-x}Ge_x$ lattice upon laser annealing. The following part describes the electrical properties as well as the structural modifications induced by the B-doping. In the final part, the objectives of the future investigations to be performed during the project are described.

2. Description of analysed samples

Different series of samples have been analysed in order to study the influence of laser annealing on $Si_{1-x}Ge_x$ and B-doped $Si_{1-x}Ge_x$ layers. Pseudomorphic $Si_{1-x}Ge_x$ layers were grown on Si (001) by Reduced Pressure Chemical Vapour Deposition in a 300 mm Epsilon 3200 tool from ASM. Before the deposition, a HF-last wet cleaning followed by an in-situ H_2 bake at 1100°C were performed on Si surfaces. For undoped samples, GeH_4, SiH_4 and Si_2H_6 were used as precursor. For B-doped samples, SiH_2Cl_2 and B_2H_6 were used as the precursor for Si and B respectively. In the case of B-doped $Si_{1-x}Ge_x$ layers, the $Si_{1-x}Ge_x$ growth was preceded by a 100 nm n-type doped Si layer to enable electrical measurement by forming a p-n junction. The laser annealing was performed with the SCREEN LT-3100 tool. For each sample, the

range of the laser energy density has been chosen in order to cover all annealing regimes from the sub-melt regime, in which the layer does not melt, to the full regime, in which the complete $Si_{1-x}Ge_x$ layer melts. The characteristics and the laser processing conditions of each sample investigated in this deliverable are presented in Table 1.

Table 1: Samples characteristics and laser processing conditions used for the annealing of $Si_{1-x}Ge_x$ layers.

Series	Ge content (%)	Thickness (nm)	Doping (cm^{-3})	Energy density range (J/cm^2)	Laser Pulse FWHM (ns)
Constant Thickness	0	30	-	1.60 – 2.60	146
	10	30	-	1.51 – 2.48	146
	20	30	-	1.40 – 2.38	146
	30	30	-	1.31 – 2.28	146
	40	30	-	1.21 – 2.18	146
Constant Ge content	30	20	-	1.11 – 2.51	160
	30	30	-	1.11 – 2.53	160
	30	45	-	1.10 – 2.51	160
B-doped	30	30	(A) 7.4×10^{19}	1.21 – 2.42	160
	30	30	(B) 1.4×10^{20}	1.21 – 2.41	160
	30	30	(C) 2.3×10^{20}	1.20 – 2.40	160

3. Investigation of undoped $Si_{1-x}Ge_x$ layers upon laser annealing

This section presents the structural and chemical modifications of $Si_{1-x}Ge_x$ layers originating from the laser thermal annealing. Depending on the energy density of the laser, different annealing regimes can be described, noted sub-melt, surface melt, partial melt and full melt. These regimes are related to the melted depth of the layer, ranging from an increase of the surface temperature to a complete melt of the thin layer. Finally, as a function of the energy densities, a complete restructuration of the initial $Si_{1-x}Ge_x$ layer can be observed. The first part details the in-depth evolution and the surface modifications of the $Si_{1-x}Ge_x$ layers. The second part concentrates on the strain state of the $Si_{1-x}Ge_x$ layers.

3.1. Characterisation of annealing regimes

3.1.1. Melt threshold of $Si_{1-x}Ge_x$ layers

During the laser thermal annealing process, the heating temperature is controlled by the energy density of the laser pulse. This means that an increase of the energy density leads to an increase of the maximum temperature reached at the sample surface. Above a certain threshold, the energy density becomes high enough to allow the melting of the $Si_{1-x}Ge_x$ layer. In Si, as the reflectivity of the liquid phase is higher than that of the solid phase [1], the transition between both phases can be highlighted by in-situ Time-Resolved Reflectometry (TRR).

Some TRR profiles recorded on $Si_{0.6}Ge_{0.4}$ layers are plotted in Figure 1.a at various energy densities. The black and red lines represent the intensity of the pulse and the measured TRR intensity as a function of time, respectively. At 1.25 J/cm^2, the slight increase of the TRR signal intensity, observed from 200 to 400 ns, is caused by the increase of the material temperature. At laser energy densities higher than 1.35 J/cm^2, a characteristic peak of the emergence of the liquid $Si_{1-x}Ge_x$ phase can be observed in TRR signals. Consequently, in the case of a 30 nm-

thick $Si_{0.6}Ge_{0.4}$ layer, the melt threshold may be close to 1.35 J/cm². For higher energy densities, the TRR intensity of the peak as well as its duration increase, indicating a deeper melt of the layer and an increase of the melt duration. At 2.00 J/cm², the TRR signal intensity reaches a plateau. This indicates that the liquid layer thickness exceeded the maximum depth probed by the laser used for TRR measurements. For instance, in polycrystalline Si thin films, the plateau appears when 20 nm of the surface thickness has been melted [1]. An analysis of the TRR signal allows to evidence the melt threshold of the sample. Such measurements were performed on all $Si_{1-x}Ge_x$ samples listed in Table 1. For instance, the evolution of the melt threshold as a function of the Ge content has been represented in Figure 1.b. This has been measured by considering TRR signals, and in addition, by considering the evolution of the surface morphology using SP2 Haze measurements. Both of these techniques are in accordance and show that, as the Ge content of the layer increased, the laser energy density required to reach the melt threshold decreased. This behaviour is consistent with the lower melt temperature of Ge (Tmelt = 938°C) compared to Si (Tmelt = 1414°C). In fact, as the Ge content in the layer increases, the melt temperature of the alloy decreases.

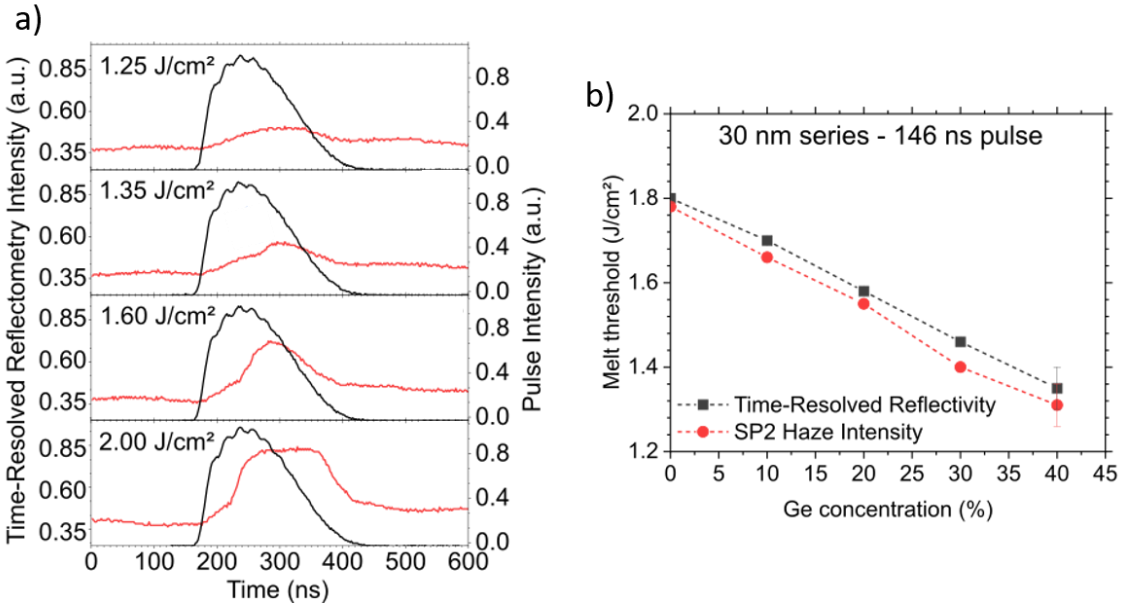

Figure 1: (a) Time-Resolved Reflectometry profiles (red line) and laser pulse signal (black line) recorded during the laser annealing on a $Si_{0.6}Ge_{0.4}$ layer at various laser energy densities. (b) Evolution of the melt threshold as a function of the Ge content in $Si_{1-x}Ge_x$ layers measured by TRR and SP2 Haze.

3.1.2. Segregation of Ge

Figure 2.a represents the ToF-SIMS Ge depth profiles from the $Si_{1-x}Ge_x$ layer surface to the Si substrate measured in 30 nm-thick $Si_{0.6}Ge_{0.4}$ layers submitted to different laser energy densities. It must be noted that variations (~3 nm) in the SiGe/Si interface depth may be observed due to layer non-uniformities. At 1.35 J/cm², close to the melt threshold (1.32 J/cm²), the Ge concentration profile remains constant all along the layer thickness and does not show any evolution compared to the reference case (i.e. as-grown). At higher energy densities, significant modifications of the Ge concentration profiles are highlighted. In these cases, the solidification following the melt of $Si_{0.6}Ge_{0.4}$ layers generated a segregation of the Ge near to the surface, leading to the Ge gradients observed for energy densities equal and higher than 1.60 J/cm². At 1.60 J/cm², the layer can be therefore separated into two part. In the melted

part, a small depletion of the Ge content is detected at a depth of 10 nm and a strong peak of Ge appears at the layer surface. The enrichment in Ge at the layer surface is a known process and it has been demonstrated that the Ge concentration can be controlled by the laser fluence [2], [3]. In fact, an increase of the energy density up to 1.81 J/cm² led to an enhancement of this phenomenon. However, the SiGe/Si interface remained unchanged, indicating that the $Si_{0.6}Ge_{0.4}$ layer has not completely melted. This type of melting will be identified as “partial melt” regime in the following parts of the deliverable. From 2.0 J/cm², the $Si_{0.6}Ge_{0.4}$ layer was close to be completely melted. At the difference with previous energy densities, no Ge depletion can be observed and the segregation mechanism caused a progressive increase of the Ge content throughout the layer. Finally, at 2.2 J/cm², the entire $Si_{0.6}Ge_{0.4}$ layer and the top of the Si substrate were melted. At this point, the Ge concentration profile shows that Ge tends to diffuse through the initial SiGe/Si interface, leading to an enlargement of the $Si_{0.6}Ge_{0.4}$ layer thickness. This melt regime will be referred as “full melt”. Similar ToF-SIMS profiles have been measured by varying the Ge content and the $Si_{1-x}Ge_x$ layer thickness as shown in Figure 2.b. In all cases the evolution of the Ge concentration along the layer as a function of the annealing regime is almost the same. The only differences correspond to the melt depth and the threshold of laser energy density required to reach the different regimes.

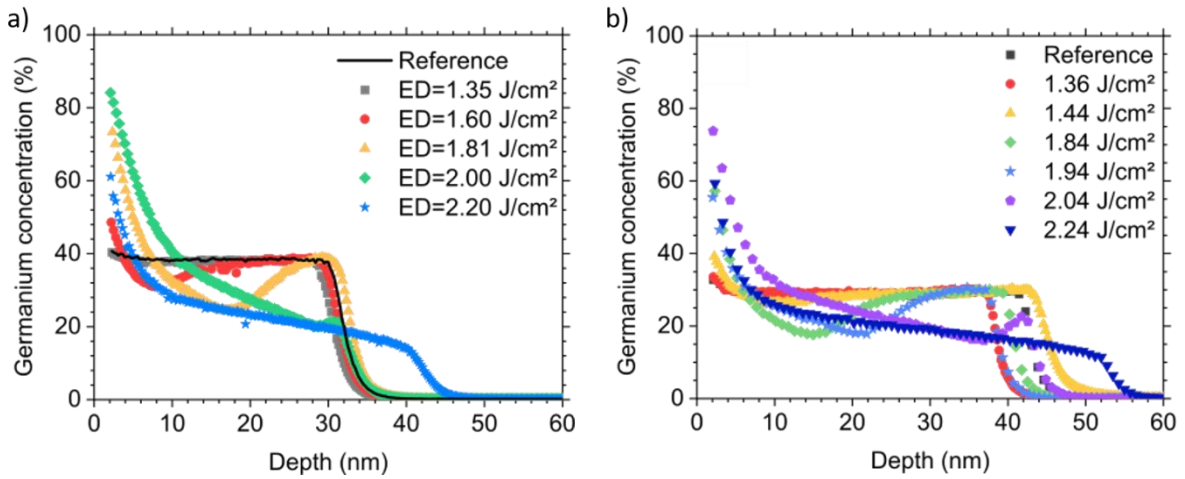

Figure 2: ToF-SIMS depth profiles of Ge concentration in (a) 30 nm thick $Si_{0.6}Ge_{0.4}$ layer and (b) 45 nm thick $Si_{0.7}Ge_{0.3}$ layer. In both cases, samples were annealed at laser energy densities ranging from 1.35 J/cm² to 2.24 J/cm².

ToF-SIMS profiles allowed to observe the evolution of the Ge concentration as a function of the annealing regimes. As strong changes of the global structure have been highlighted, it can be useful to investigate the evolution of the nanostructure for these same samples. For this purpose, STEM-HAADF micrographs of $Si_{0.6}Ge_{0.4}$ samples annealed with laser energy densities ranging from 1.60 to 2.20 J/cm² are represented in Figure 3. In the STEM HAADF mode, the signal intensity is proportional to the atomic number Z. By consequence, in Figure 3 Ge-rich areas are represented with a brighter contrast. It allowed to clearly differentiate $Si_{0.6}Ge_{0.4}$ layers and Si substrate as well as the Ge segregation inside the $Si_{0.6}Ge_{0.4}$ layer, and to characterize the different annealing regimes.

Unlike the ToF-SIMS profiles, the STEM-HAADF micrographs allowed to identify the formation of nanostructures at the surface of the sample. A new melt regime can be defined as a “surface melt” regime. In fact, as it appears on Figure 3.a, at 1.60 J/cm² the layer is non-homogeneously melted allowing to identify the formation of surface nanostructures (up to 70 nm wide and 6 nm

high). These structures are separated by unmelted areas. A more detailed characterisation of this surface structuration will be done in the following sections. At 1.81 J/cm², the $Si_{0.6}Ge_{0.4}$ layer surface is entirely melted. The difference of contrast obtained on STEM-HAADF is consistent with the Ge depth profiles (Figure 2.a). In fact, in Figure 3.b, the unmelted area in the lower part of the $Si_{0.6}Ge_{0.4}$ layer appears in a bright uniform contrast, corresponding to a constant Ge concentration. In the upper part, the darker area shows the depletion of Ge concentration caused by its segregation. Finally, the contrast becomes brighter near to the surface due to segregation [2], [3]. The difference of contrast between unmelted and melted areas was high enough to easily identify the position of the liquid/solid (l/s) corresponding to the maximum melt depth. It is interesting to note that this l/s interface presents some kind of roughness which may be linked to the nanostructuration appearing during the surface melt regime. As observed on ToF-SIMS profiles, at 2.00 J/cm² and 2.20 J/cm², the melt depth increases until it exceeds the initial thickness of the $Si_{0.6}Ge_{0.4}$ layer. It highlights that when the melt depth approaches the SiGe/Si substrate interface, the l/s interface flattens. The flattening of the l/s interface is probably due to the higher melt temperature of Si. Even if the melting of the $Si_{0.6}Ge_{0.4}$ proceeds in an “inhomogeneous” way (due to the roughness of the l/s interface, cf. Figure 3.b), the $Si_{0.6}Ge_{0.4}$ layer must completely melt before the melt of the Si substrate can start.

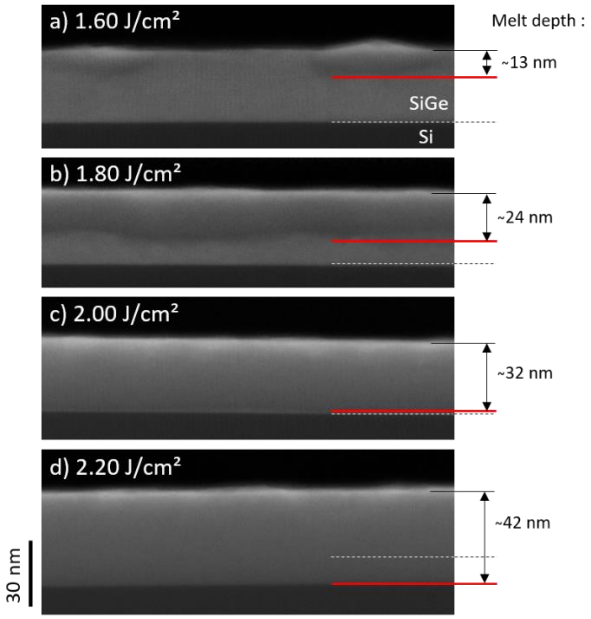

Figure 3: STEM-HAADF micrographs recorded on a 30 nm-thick $Si_{0.6}Ge_{0.4}$ layer at various laser energy densities. Bright contrasts evidence the Ge-rich phases. Dotted white lines represent the initial position of SiGe/Si substrate interface and red lines show the maximum melt depth for each annealing condition.

3.1.3. Energy density range of melt regimes

Finally, from the previous investigations, four distinct melt regimes were defined concerning the laser annealing of $Si_{1-x}Ge_x$ thin layers. Regardless of the $Si_{1-x}Ge_x$ characteristics, the sub-melt, surface melt, partial melt and full melt regimes can be observed. However, the thresholds of energy density, which must be reached to switch between the melt regimes, depend on the layer composition and/or thickness. The corresponding range of each regime, in terms of energy densities, for all analysed samples is presented in Figure 4.

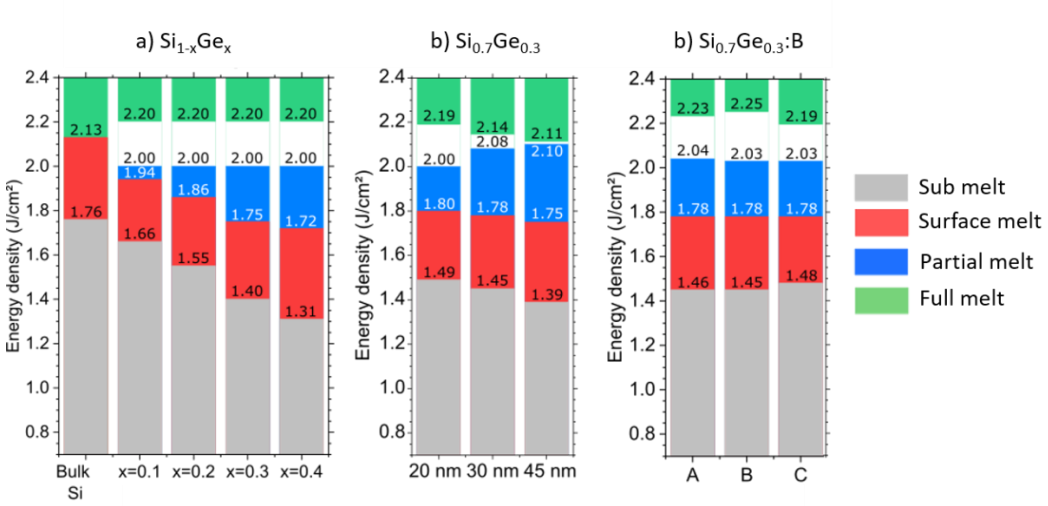

Figure 4: Summary of the laser annealing regimes observed for the different analysed series. (a) 30 nm thick $Si_{0.6}Ge_{0.4}$ layer depending on the Ge content. (b) $Si_{0.7}Ge_{0.3}$ layer as a function of the layer thickness. (c) B-doped $Si_{0.7}Ge_{0.3}$ layer.

3.2. Surface structuration

As seen on Figure 3.a, for laser energy densities slightly above the melt threshold (i.e. in the surface melt regime), instead of observing the formation of a continuous liquid layer, isolated nanostructures grew at the surface of the $Si_{0.6}Ge_{0.4}$ layer. These isolated structures originate from the inhomogeneous melt of the layer surface. To investigate these structures and their evolution, AFM scans provided the best insight. 1×1 µm² AFM scans corresponding to the beginning of the surface melt regime are presented in Figure 5 as a function of the Ge content. In all cases, the laser energy density has been chosen from the melt thresholds determined by TRR measurements presented in Figure 1.b. The different AFM scans evidence that the surface-melt regime occurs regardless of the Ge content. This proves that the local melt and the formation of such surface nanostructures are not specifically related to the presence of Ge or to the alloy properties. It is interesting to note a shape modification according to the Ge content. In fact, if these nanostructures grew in a square-shape in bulk Si, the increase of Ge content tends to turn them into a cross-shape which seems to extend preferably along the <1 0 0> crystallographic directions. However, it clearly appears that the height and width of these nanostructures strongly decrease as the Ge content increases. The growth of surface structures after laser annealing has also been observed in the early stages of melting in both Ge and Si surfaces [4], [5]. These structures have been interpreted as a consequence of a local melt of the surface and may originate from the nucleation occurring during the first-order solid-liquid phase transition.

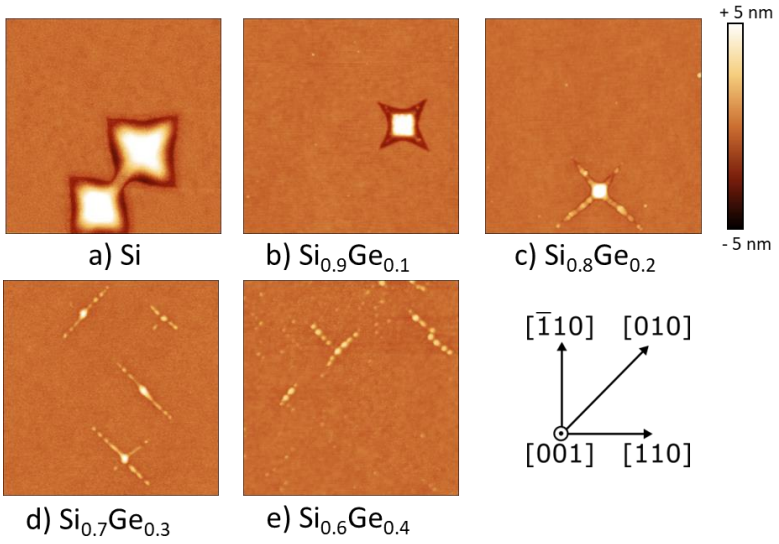

Figure 5: 1×1 µm² AFM scans obtained after laser annealing of $Si_{1-x}Ge_x$ layers at (a) 1.78 J/cm², (b) 1.66 J/cm², (c) 1.55 J/cm², (d) 1.45 J/cm² and (e) 1.32 J/cm². These values correspond to the melt threshold determined on Figure 1.b.

The AFM images displayed in Figure 6.a show the evolution of these nanostructures as a function of the laser energy density in $Si_{0.6}Ge_{0.4}$. As described above, in the first step of the surface melt, at 1.32 J/cm², AFM images evidence the formation of cross-shaped nanostructures elongated along the <1 0 0> crystallographic directions. By increasing the laser energy density, the nanostructures become more numerous and start to merge. At 1.61 J/cm², around 50 % of the surface is covered by small islands with a mean height of 4 nm and a mean width of 80 nm. This confirms that these nanostructures detected by AFM are the ones observed in Figure 3.a, on STEM-HAADF micrographs. The formation of such structures is probably due to the progressive melting and covering of the surface by isolated melted islands. At 1.80 J/cm² and for higher energy densities, the surface starts to melt completely which leads to the formation of a continuous liquid layer covering the entire surface. At this point, the surface tends to flatten but still continues to exhibit some roughness. It is interesting to note that in the literature, similar surface structuration have been evidenced and revealed some kind of periodicity [6], whereas, in this case, no specific order could be highlighted. The evolution of the surface coverage ratio as a function of the laser energy density is plotted in Figure 6.b. Regardless of the Ge content, there is a linear increase of the covered surface as a function of the energy density. The energy interval between 0% and 100% surface coverage increases with Ge content. This suggests that the nucleation rate of the surface islands or their growth rate decrease with higher Ge contents.

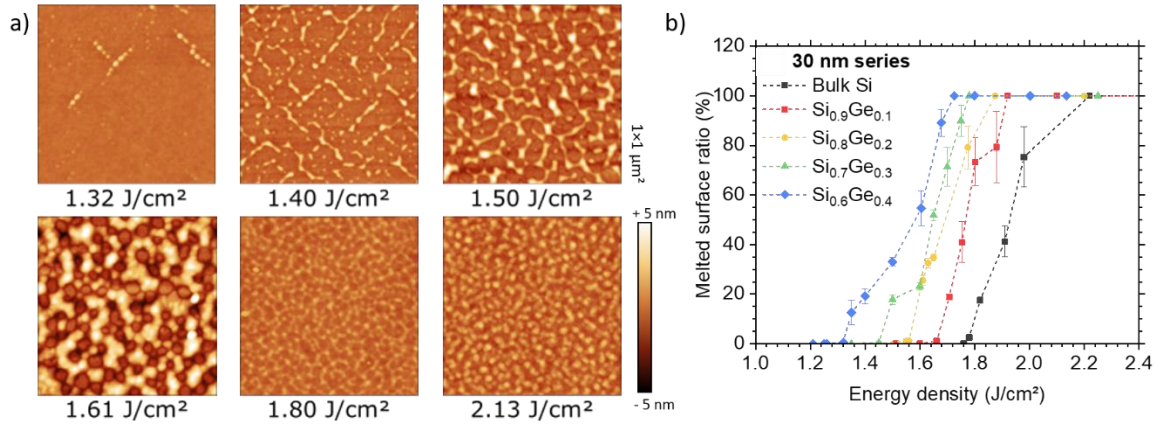

Figure 6: (a) 1×1 µm² AFM scans recorded on a 30 nm thick $Si_{0.6}Ge_{0.4}$ layer at different laser energy densities. (b) Evolution of the melted surface coverage as a function of the laser energy density for all Ge content.

3.3. Strain Relaxation of pseudomorphic $Si_{1-x}Ge_x$ layer

3.3.1. Dependence on the annealing regime

For the different annealing regimes of the $Si_{0.6}Ge_{0.4}$ layer, the degree of strain relaxation has been calculated on the basis of Reciprocal Space Maps (RSM) around the (224) diffraction order. These measurements enabled to identify the position of the $Si_{0.6}Ge_{0.4}$ spot in the reciprocal space relatively to the Si spot, and to measure its coordinates in the reciprocal space. As this corresponds to an asymmetrical measurement, the position of the spot along the q_x axis is indicative of the relaxation and should be vertically aligned with the Si spot for a strained layer. The RSMs measured on $Si_{0.6}Ge_{0.4}$ for the four annealing regimes are represented in Figure 7. At 1.20 J/cm², i.e. in the sub-melt regime, the vertical alignment of the q_x spot with the Si spot evidences the pseudomorphic nature of the $Si_{0.6}Ge_{0.4}$ layer. For higher laser energy densities, whether it be for surface melt or partial melt regimes, Figures 7.b and 7.c show wider and left shifted SiGe peaks. Such displacement toward the left indicates a relaxation of the initially strained layer. At 2.00 J/cm², i.e. in the full melt regime, two distinct spots can be attributed to the SiGe peak. The presence of two spots may be due to the separation of the initial layer into two parts. The first one is vertically aligned with the spot, showing the presence of a strained part. The second one is more diffused and is left-shifted, indicating the presence of a partially relaxed part.

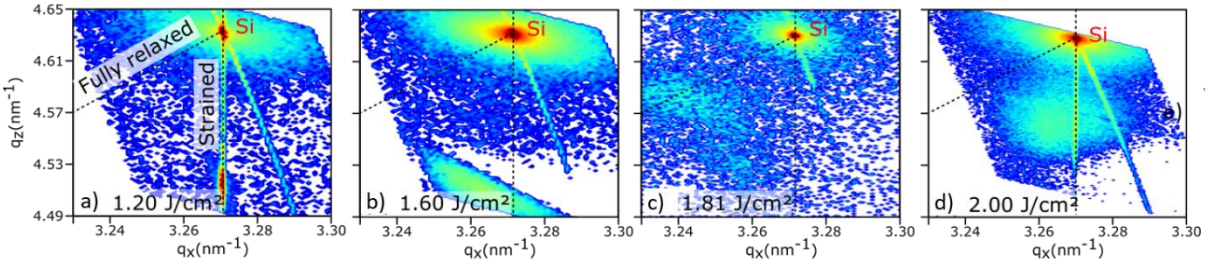

Figure 7: Reciprocal Space Maps along the (224) direction on a 30 nm thick $Si_{0.6}Ge_{0.4}$ layer laser annealed at (a) 1.20 J/cm², (b) 1.60 J/cm², (c) 1.81 J/cm² and (d) 2.00 J/cm². Vertical and tilted dotted lines represent the theoretical position of the SiGe spot for a fully strained and a fully relaxed layer respectively.

The degree of strain relaxation can be estimated using the following expression [7]:

$$(1) \quad R = \frac{a^{/\!/}_{SiGe} - a_{Si}}{a^{0}_{SiGe} - a_{Si}}$$

Where $a^{/\!/}_{SiGe}$ is the in-plane lattice parameter of the strained SiGe layer, a^{0}_{SiGe} is the lattice parameter of completely relaxed SiGe and a_{Si} is the lattice parameter of relaxed Si ($a_{Si} = 5.43105$ Å). The calculated R coefficients have been plotted in Figure 8 as a function of the laser energy densities and depending on the Ge content. In parallel, Dark-Field TEM (DF-TEM) micrographs have been recorded from samples annealed at energies from 1.60 J/cm² to 2.20 J/cm² for $Si_{0.6}Ge_{0.4}$ and are shown in Figure 9. Usually DF-TEM micrographs allow to highlight the presence of defects in the observed material.

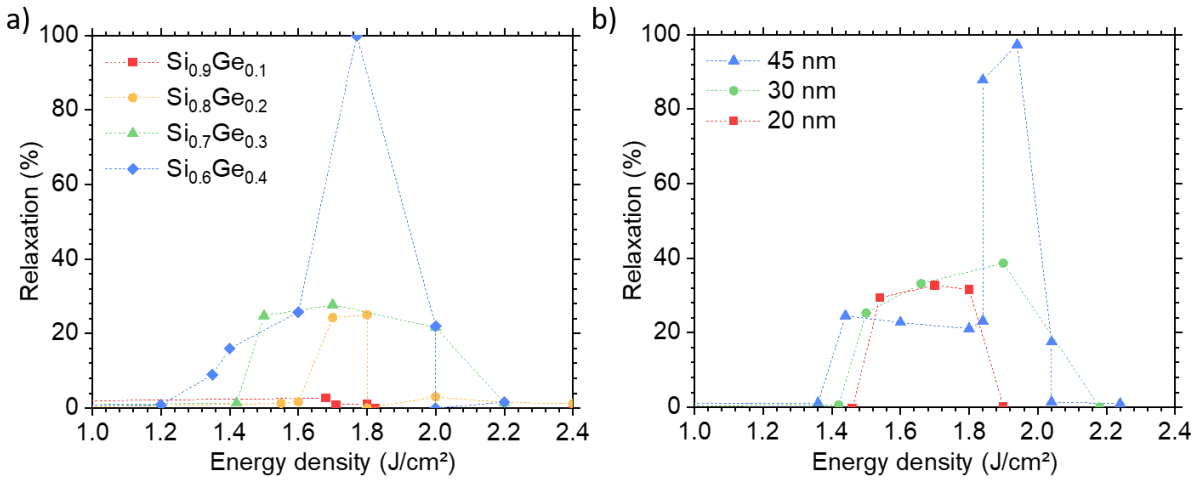

Figure 8: Evolution of the degree of relaxation as a function of the laser energy density depending on (a) the Ge content in 30 nm-thick layers and (b) the thickness of $Si_{0.7}Ge_{0.3}$ layers. These data were extracted from RSM datas.

In the case of $Si_{0.6}Ge_{0.4}$, until the end of the sub-melt regime, the layer remains pseudomorphic. In the surface melt regime, a partial relaxation of the $Si_{0.6}Ge_{0.4}$ layer starts to occur. Then, the degree of relaxation increases from R = 10% at 1.35 J/cm² to R = 26% at 1.60 J/cm². The DF-TEM presented in Figure 9.a evidences the presence of defects over the whole thickness of the layer annealed at 1.60 J/cm². The observed defects consist mostly of (111) staking faults located beneath the melted islands and of misfit dislocations parallel to the SiGe interface. After a partial melt, at 1.80 J/cm² the $Si_{0.6}Ge_{0.4}$ layer is totally relaxed. DF-TEM images showed in Figure 9.b seem to confirm this result, evidencing an increase of the defects density including staking faults and misfit dislocations. At 2.00 J/cm², which represents the limit between the partial and full melt regimes, considering the RSM presented in Figure 7, the annealing process should lead to the formation of two parts, a fully strained part and a partially relaxed part (R = 22%). The DF-TEM micrographs (Figure 9.c) highlights the presence of a defects band confined within a surface layer of about 15 nm thickness, while the rest of the layer, down to the SiGe/Si substrate interface is defect free. Then, in this particular case, a bilayer structure made of a fully strained part in depth, and a partially relaxed part at the top of the layer is formed. Similar results can be observed at higher energy densities (Figure 9.d), however the degree of strain relaxation could not be measured in this case because of the too low intensities

of the XRD signals. These strain relaxation measurements have been performed for all Ge contents and depending on the layer thickness (Figure 8.a and 8.b). All samples were found to be fully strained until the surface melt regime is reached independently of the Ge content or layer thickness. However, if the strain relaxation in $Si_{0.8}Ge_{0.2}$ and $Si_{0.7}Ge_{0.3}$ seems to occur as described above in $Si_{0.6}Ge_{0.4}$ for the different melt regimes, it is interesting to note that in the case of $Si_{0.9}Ge_{0.1}$, the SiGe layer did not show any strain relaxation regardless of the annealing regime.

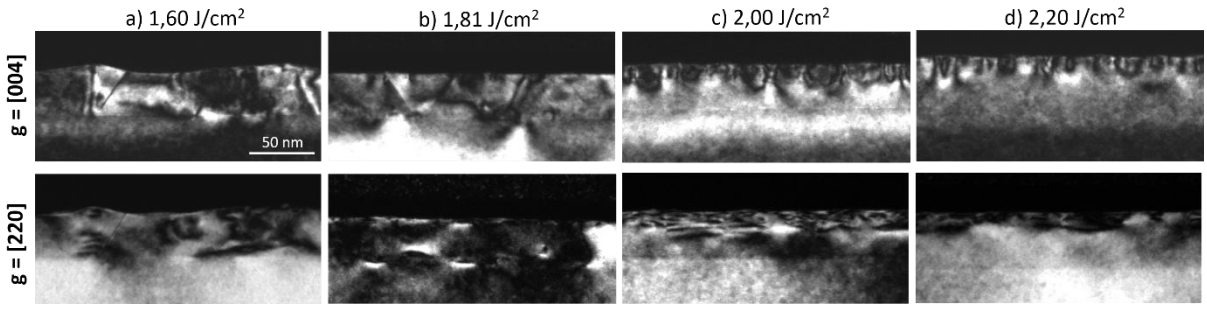

Figure 9: Cross-sectional Dark-Field TEM micrographs recorded in 30 nm-thick $Si_{0.6}Ge_{0.4}$ layer laser annealed at various energy densities. In each case, observations were performed using g = [004] and g = [220] as diffracting vectors.

3.3.2. Origin of the strain relaxation

The results observed on the formation of strain relieving defects may be qualitatively explained thanks to STEM-HAADF images (Figure 3), by considering the impact of the l/s interface roughness formed during the solidification mechanism. In fact, combining DF-TEM and STEM-HAADF images, it can be evidenced that a rough l/s interface leads to the formation of more defects. The formation of strain relieving defects has already been observed during the Low Temperature Solid Phase Epitaxial Regrowth (LT-SPER) of amorphized SiGe/Si epilayers, for which an elastic energy-driven relaxation mechanism was proposed [8]. During the recrystallization, it was shown that the initially flat amorphous/crystalline interface progressively transformed into a faceted one along {111} planes. The interface roughness increased proportionally to the Ge content and favoured the formation of strain relieving defects (staking faults, misfit dislocations …), provided that the elastic energy density stored in the layer exceeded a critical value. In the case of $Si_{1-x}Ge_x$ layers obtained by ion implantation, the critical value inducing the strain relaxation was estimated at 300 mJ/m² [9].

In the case investigated here, some samples have shown a solidification mechanism starting inside the $Si_{1-x}Ge_x$ layer and resulting in the formation of strain relieving defects throughout the whole layer (Figure 8 and 9) independently of the Ge content. In fact, as observed on STEM-HAADF images in surface and partial melt regimes (Figure 3.a and 3.b), the inhomogeneous melting of the layer (noted by the presence of a rough l/s interface) should induce a regrowth along different crystallographic directions, favouring the formation of strain relieving defects (seen in Figure 9.a and 9.b). However, in samples annealed at higher energy densities (at 2.00 J/cm² and 2.20 J/cm²), strain relaxation seems to follow the elastic energy-driven relaxation mechanism. In fact, at the end of the partial melt (and also in full melt regimes), the solidification starts from a flat interface resulting in a defect free bottom layer covered by a thin layer containing the strain relieving defects. It should be inferred that the formation of these defects occurs when the elastic energy stored in the regrown layer reaches a critical value.

The calculation of the elastic energy stored in a SiGe layer with a constant Ge content can be found in ref [10]. This relation has been slightly modified to take into account the gradient of Ge observed in the samples investigated here (Figure 2). The elastic energy stored can be expressed as:

$$(2) \qquad E = \int_{z=surface}^{z=layer\ thickness} B \cdot \varepsilon(z)^2 \cdot dz$$

$$(3) \qquad B = 2\mu(z) \cdot \frac{1+\nu(z)}{1-\nu(z)}$$

Where $\varepsilon(z)$ is the strain, $\mu(z)$ the shear modulus and $\nu(z)$ the Poisson's ratio. All of these parameters are dependent on the Ge content in the layer and thus on the depth. In each case, the Ge content has been determined by modelling the experimental Ge profiles obtained from ToF-SIMS or EDX measurements.

For each sample which appeared to follow the elastic energy-driven relaxation mechanism (i.e. corresponding to an annealing in the end of partial melt or full melt regimes), the elastic energy has been computed and plotted in Figure 10.a. Here, solid symbols correspond to fully strained layers, whereas empty ones correspond to layer exhibiting the bilayer structure. Based on these results, the critical value of elastic energy inducing the formation of strain relieving defects can be estimated at around 750 mJ/m². This value is way higher than the threshold determined in the case of ion beam synthesized SiGe layers (300 mJ/m²) [9]. Therefore, a fully pseudomorphic regrowth during the solidification mechanism is available only if the elastic energy stored in the layer is lower than 750 mJ/m². In these annealing regimes the elastic energy calculations are in accordance with the results obtained on RSMs and DF-TEM images. Moreover, results obtained in the literature for thicker $Si_{1-x}Ge_x$ layer and with a shorter laser pulse (fully strained, presenting an elastic energy density of 700 mJ/m²) are consistent with the observed behaviour [11].

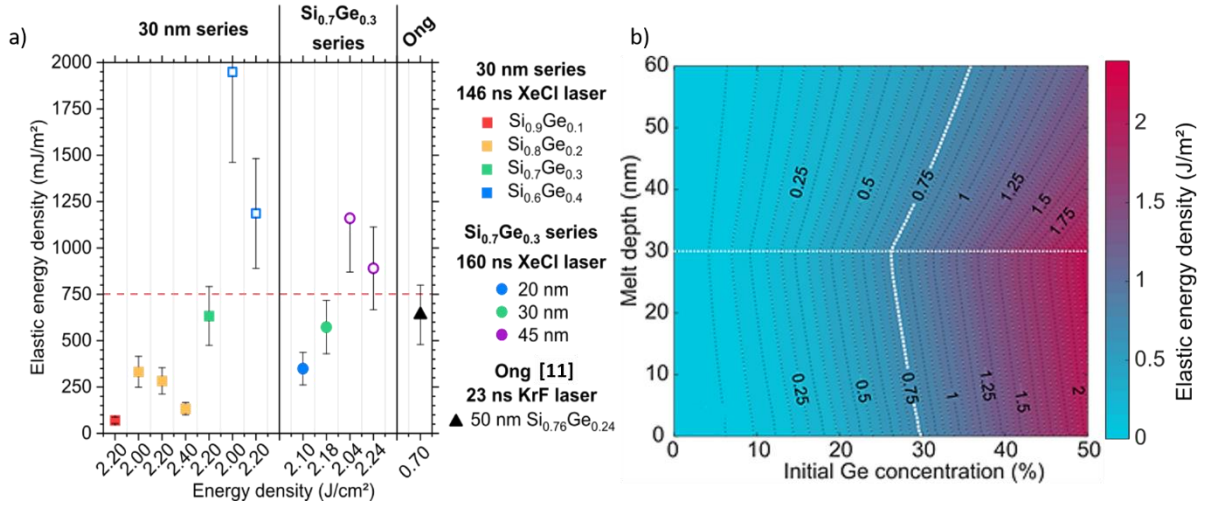

Figure 10: (a) Total elastic energy density calculated in SiGe layers following the equation (2). The calculation was performed only on sample showing a smooth l/s interface. Open symbols and full symbols correspond respectively to $Si_{1-x}Ge_x$ layer with a bilayer structure and fully strained layer. (b) Colour maps of simulated elastic energy densities for various Ge content and at different melt depths. In both figures, dotted line highlights the estimated critical value at 750 mJ/m².

Ge concentration profiles have been simulated as a function of the annealing conditions and Ge content. Then, for each simulated profile, the stored elastic energy can be calculated following equation (2). One of this simulation is presented in a form of colour map in Figure 10.b. It was performed in the case of 30 nm-thick $Si_{1-x}Ge_x$ layers, for Ge content ranging from 0 to 50 % and melt depth ranging from 0 to 60 nm. Regardless of the Ge content, the evolution of the elastic energy density follows the same trend. For melt depths below the layer thickness, the elastic energy density increases due to the Ge redistribution near to the surface. For melt depths beyond the layer thickness, the Ge gradient is less important and counter-balanced by the Ge redistribution over a thicker area, leading to an overall decrease of the stored elastic energy density. The elastic energy threshold has been highlighted by the thick white dotted line. Considering a pure elastic energy-driven relaxation mechanism, some of these results are well in accordance with the observations made on RSMs and DF-TEM images. In fact, regardless of the laser energy density, $Si_{0.9}Ge_{0.1}$ layer remains fully strained, corresponding to low stored elastic energy density values, while, in partially or fully relaxed layer (i.e. $Si_{0.6}Ge_{0.4}$ and $Si_{0.7}Ge_{0.3}$ in surface and partial melt regimes), Figure 10.b shows that the computed elastic energy density is well above the critical value in agreement with the observed relaxation for these samples. In contrast, in some other cases, such as the $Si_{0.8}Ge_{0.2}$ samples annealed in the partial melt regime (i.e. from 1.6 to 1.8 J/cm²) a strain relaxation around 20 % was measured, although the stored elastic energy density is systematically lower than the critical value. This is probably linked to the roughness of l/s interface typically observed upon surface and partial melt regimes. Detailed investigations about this behaviour, including a quantitative evaluation of the l/s roughness as a function of the annealing conditions, are planned within the MUNDFAB work plan and will be reported in future reports. They are expected to allow a clear understanding of the relation between the l/s roughness, elastic energy and defects formation during laser annealing.

4. Boron doping of $Si_{1-x}Ge_x$ layer

In this section, the first results of B-doped $Si_{0.7}Ge_{0.3}$ layers are described. Three B-doped layers have been investigated corresponding to three different boron atomic concentrations (7.4×10^{19}, 1.4×10^{20} and 2.3×10^{20} at.cm^{-3}, cf. D3.3). In the following sections these samples will be noted A, B and C respectively. The first part describes the strain relaxation of B-doped samples, while the second part concentrates on their electrical properties.

4.1. Strain relaxation in Boron doped samples.

For all three Boron concentrations, the transition from one annealing regime to the other occurred at the same laser energy densities which are closed to the one determined for undoped layers (Figure 4). Figure 11.a compares the evolution of the degree of relaxation in each case as a function of the laser energy densities. As seen in the previous part, the relaxation of the undoped layer (≈ 30%) is induced by the presence of strain relieving defects linked to the l/s interface roughness in the surface and partial melt regimes (i.e. from 1.4 to 2.0 J/cm²). At higher energy densities, the l/s interface flattens and the $Si_{1-x}Ge_x$ layer returns to a pseudomorphic state.

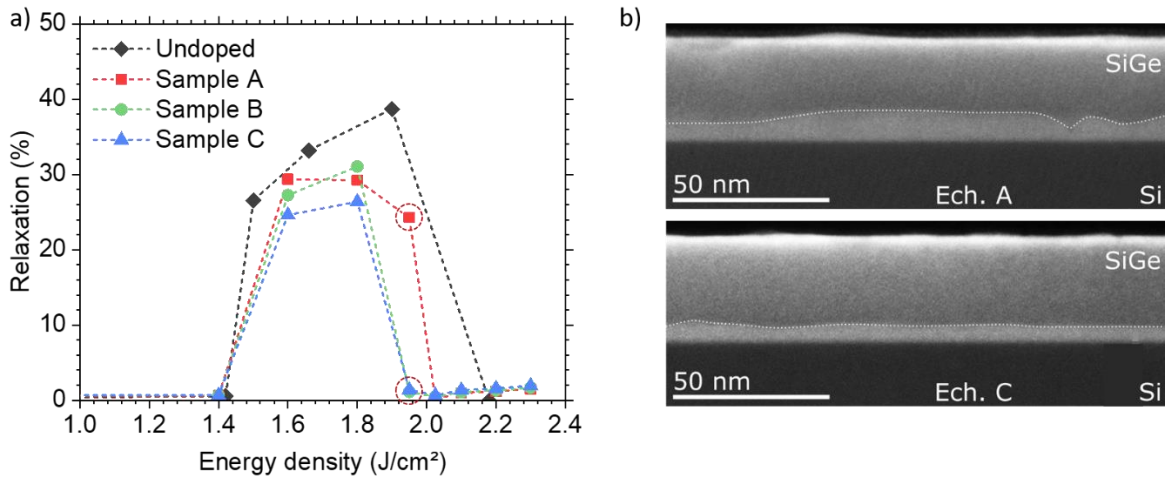

Figure 11: (a) Evolution of the degree of relaxation for undoped and B-doped 30-nm thick $Si_{0.7}Ge_{0.3}$ layers laser annealed at different energy densities. (b) STEM-HAADF micrographs recorded in samples A and C laser annealed with an energy density of 1.95 J/cm². Dotted lines highlight the l/s interface.

In the B-doped samples, this evolution was slightly different. First, all B-doped layers present a lower degree of relaxation than the undoped one. By increasing the dopant concentration, the relaxation level decreases, reaching its minimum value for sample C. This may be directly linked to the inclusion of boron atoms in the lattice. In fact, due to the lower covalent radius of boron, the presence of boron results in a reduction of the B-doped $Si_{0.7}Ge_{0.3}$ lattice parameter compared to the undoped $Si_{0.7}Ge_{0.3}$. It may cause a strain compensation and reduce the stored elastic energy density. Second, at 1.95 J/cm², both samples B and C return to a fully strained state whereas sample A exhibits a relaxation near 25 %. This observation was unexpected as this energy density does not allow to reach the full melt regime, which is the only case in which the lattice is fully strained in undoped layers. To investigate this particularity, STEM-HAADF have been performed for B-doped sample annealed at 1.95 J/cm², and the results are shown in Figure 11.b for the sample A and C. In both samples, the maximum melt depth is very similar, however, the roughness of the l/s interface is clearly different. As in the case of undoped layers, the presence of a rough l/s interface seems to facilitate the formation of strain relieving defects in sample A, explaining the relaxation measured at 1.95 J/cm². On the contrary, the smooth l/s interface observed in sample C results in a fully strained structure, suggesting that in this case the stored elastic energy density becomes lower than the threshold value for relaxation. Indeed, the introduction of a large boron concentration in the layer is expected to reduce the elastic energy density compared to the undoped case, by decreasing it below the critical value.

4.2. Electrical properties

The electrical properties of B-doped $Si_{0.7}Ge_{0.3}$ layers were investigated by four-point probe measurements to obtain the sheet resistance and were completed by Hall effect measurements. The analysis of the three as-grown samples (i.e. before laser annealing) is described in deliverable D3.3. In particular, by combining Hall effect measurements and SIMS chemical profiles (presented in Fig. 12), it was possible to establish that only in sample A (doped with the lowest Boron concentration of 7.4×10^{19} cm^{-3}) the totality of the Boron atoms was electrically active. In contrast, in samples B and C, doped with higher Boron concentrations (1.4×10^{20} cm^{-3} and 2.3×10^{20} cm^{-3}, respectively), only a partial electrical activation was achieved (~80% and ~60%, respectively).

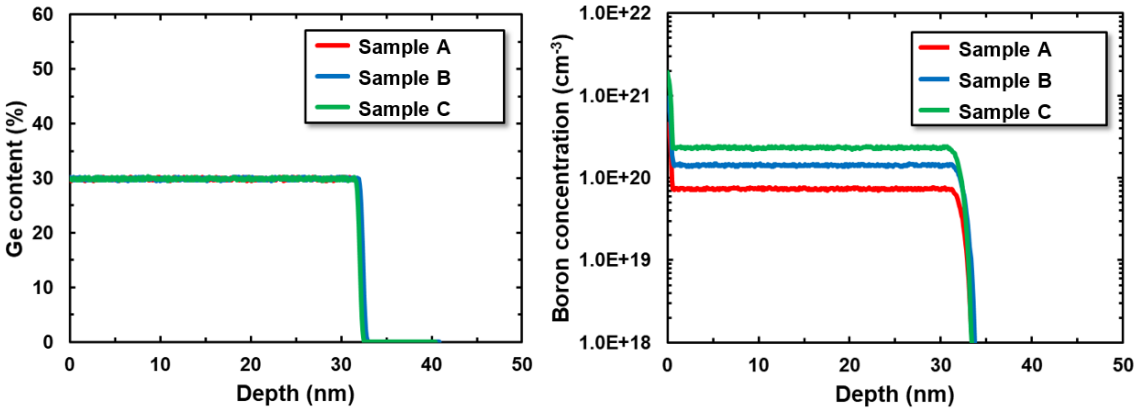

Figure 12: Germanium **(a)** and boron **(b)** concentration profiles as a function of depth obtained by SIMS for 30 nm-thick *in-situ* boron-doped $Si_{0.7}Ge_{0.3}$ layers at different boron concentration levels: $7.4x10^{19}$ cm^{-3} (sample A, red); $1.4x10^{20}$ cm^{-3} (sample B, blue); $2.3x10^{20}$ cm^{-3} (sample C, green).

The evolution of the sheet resistance as a function of the laser energy density, measured by four-point probes and Hall measurements is displayed in Figure 13.a for samples A, B and C. The dotted lines correspond to the average sheet resistance measured before laser annealing. It must be noticed that both measurements match well in all cases. In the sub melt regime (up to 1.4 J/cm²), no changes can be highlighted in the sheet resistance compared to the initial state, indicating that this melt regime did not cause any modifications in the layer. In the surface and partial melt regimes (from 1.4 J/cm² to 2.0 J/cm²), the behaviour differs between the samples. For samples A and B, a degradation of the sheet resistance occurs at the beginning of the surface melt and continues until the end of the partial melt regime. However, in this same range of annealing, for the sample C the effect is reversed and a progressive decrease of the sheet resistance is observed. As soon as the full melt is reached, all samples exhibit an abrupt improvement of the sheet resistance, which tends to stabilize below the initial level for samples B and C, and above it for the sample A.

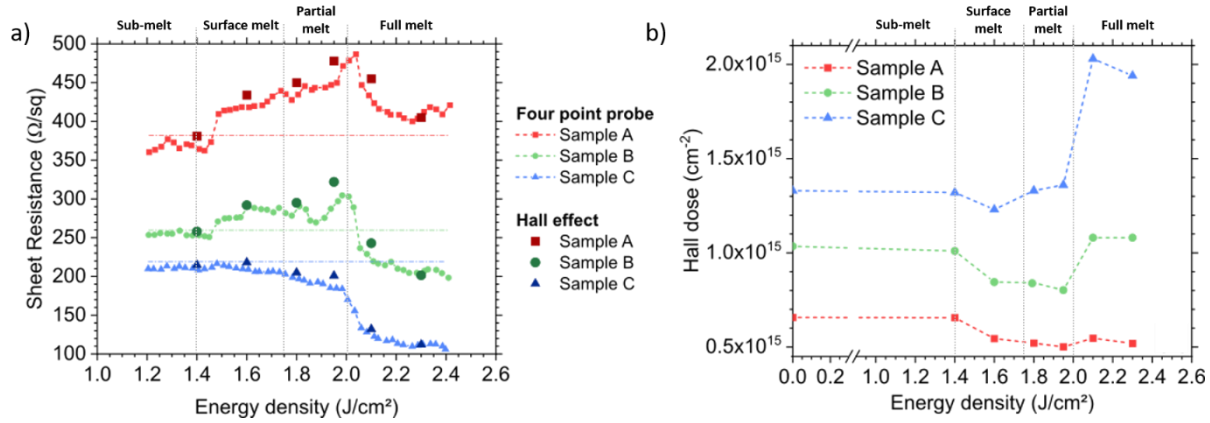

Figure 13: Evolution of (a) sheet resistance and (b) Hall dose in B-doped $Si_{1-x}Ge_x$ layers as a function of the laser energy density. Vertical lines allow to separate the different melting regimes.

The Hall dose was measured for each sample depending on the laser energy density. The results are presented in Figure 13.b. For the sample A, the Hall dose decreases once the melt threshold is reached and remains below the initial value (0.65×10^{15} cm^{-2}) in partial as in full

melt regimes. For the sample B, the same behaviour occurs in surface and partial melt. However, at the end of the partial melt (2.0 J/cm²), the Hall dose increases and becomes slightly higher than the initial value (1.1×10^{15} cm^{-2}). In the section 3.1, it has been evidenced that, from the surface melt to the partial melt regime, both samples were partially relaxed. This relaxation is triggered by the formation of crystalline defects in the B-doped $Si_{0.7}Ge_{0.3}$ layer, which are expected to deteriorate the transport properties of the layer [12]. Indeed, it has already been demonstrated that the presence of dislocations in a relaxed $Si_{1-x}Ge_x$ layer leads to the formation of traps or recombination centres for holes [13]. At the end of the partial melt regime, both layers return to a pseudomorphic state, then, the disappearance of crystalline defects leads to the increase of Hall dose. Finally, in sample C, the evolution of the Hall dose is different. In this case, the Hall dose remains barely stable until the full melt is reached, while it strongly increases at higher energy densities. The same phenomenon as the one described above may occur in sample C. However, in this sample, a large fraction of the boron atoms was found to be electrically inactive at the initial state (~40%). Then, the stable Hall dose measured throughout the partial melt regime suggests that a part of these boron atoms can be activated during the laser anneal, therefore allowing to compensate the deterioration due to carriers trapped at relaxation-induced defects.

5. Prospects of future investigations

In this final section, future experimental studies that might contribute to elucidate the various mechanisms investigated in strained SiGe layers submitted to melt laser annealing will be briefly discussed. They are expected to improve the overall understanding of the interplay occurring between l/s interface roughness, strain relaxation and defect formation and provide valuable data for further improvement of predictive models developed in MUNDFAB.

5.1. Quantification of l/s interface roughness

The observations of STEM-HAADF micrographs of $Si_{1-x}Ge_x$ layers allowed to evidence the presence of a rough l/s interface which tends to flattens by increasing the laser energy density, when the melt depth reaches the Si substrate. Although the origin of this roughness can be associated to the nanostructuration of the surface during the so-called surface melt regime, at this point this phenomenon is not completely understood. As reminded in Figure 14.a, it has been evidenced that in the case of a 30 nm-thick $Si_{0.6}Ge_{0.4}$ layer laser annealed at 1.8 J/cm², the presence of a rough l/s interface induced the complete relaxation of the layer due to the formation of strain relieving defects. By comparison, same investigations performed on a 30 nm-thick $Si_{0.8}Ge_{0.2}$ layer laser annealed at 1.925 J/cm² (Figure 14.b), in which only negligible relaxation has been evidenced on RSMs (Figure 8.a), show that the absence of numerous strain relieving defects must be linked to the smooth l/s interface observed. This indicates that, on one side, the formation of strain relieving defects is strongly correlated to the roughness of the l/s interface, and on the other side, the roughness is not only linked to the melt depth, as similar depths have been measured in both samples. Finally, different parameters (i.e. Ge content, B-doping, melt depth …) should be involved in the evolution of the l/s interface roughness. In order to identify the origin and the influence of this roughness on the SiGe layer properties (especially concerning the relaxation), it will be necessary to define and quantify a roughness parameter and investigate its evolution as a function of SiGe layer characteristics.

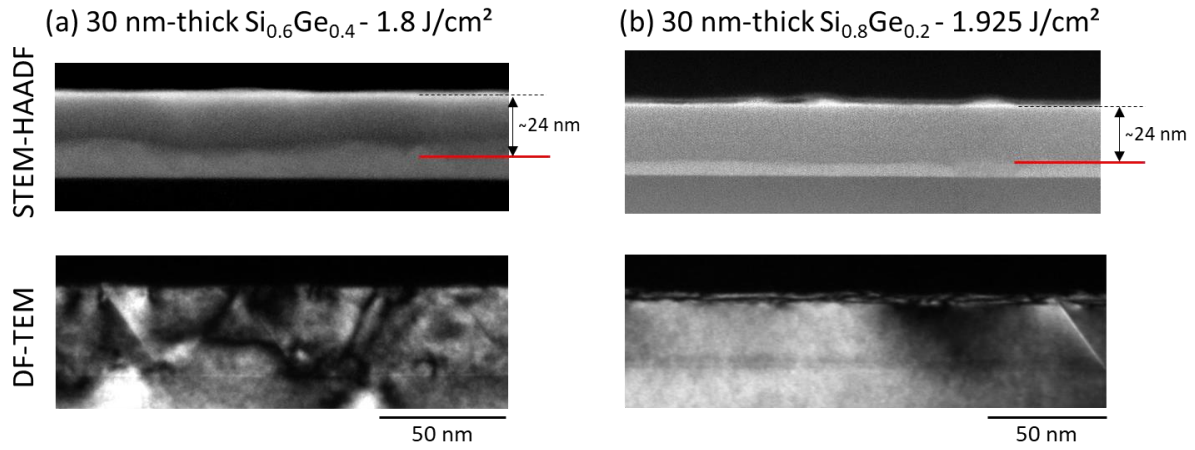

Figure 14: STEM-HAADF and DF-TEM images recorded in (a) 30 nm-thick $Si_{0.6}Ge_{0.4}$ layer laser annealed at 1.8 J/cm² and (b) 30 nm-thick $Si_{0.8}Ge_{0.2}$ layer laser annealed at 1.925 J/cm². Red lines represent the mean melt depth.

5.2. Fully relaxed initial layer

All samples investigated in this deliverable were grown on Si (001) and were fully strained prior to laser annealing. However, it has been evidenced that in some conditions, especially in surface melt and partial melt regimes (i.e. when the l/s interface is rough), the pseudomorphic SiGe layer tends to relax, inducing the formation of unwanted strain relieving defects all along the layer. A mean to understand the connection between the l/s interface roughness and the formation of defects in the layer, should be to remove the initial strain state of the layer. Then, it may be interesting to make similar investigations in initially fully relaxed $Si_{1-x}Ge_x$ layers, in order to observe jointly the evolution of the l/s interface roughness and the formation or not of defects in these relaxed layers. Such experiments will be carried out using the new set of wafers fabricated at CEA-Leti (cf. D3.2), which include a subset of fully relaxed SiGe layers with a Ge content of 20% and 50%.

5.3. Origin and characteristics of surface islands

As explained previously, the presence of a rough l/s interface in $Si_{1-x}Ge_x$ layers laser annealed in the partial melt regime may be directly linked to the initial surface structuration, originating from the first steps of surface melt regime. During this annealing, an inhomogeneous melt of the surface induces the formation of islands, in which a gradient of Ge towards the surface can be observed as in partial melt regime. Apart from these islands, the rest of the sample remains unmelted. In bulk Si as in pure Ge, the recrystallization after the laser annealing in surface melt occurs in specific crystallographic directions and results in the formation of square faceted nanostructures. In contrast, the surface islands exhibit a cross-shape in strained SiGe layers. The origin of this shape modification may be due to the strain relaxation that might occur at the lateral interfaces of the surface liquid droplets during the early stages of the surface melt regime. Again, it is expected that performing a similar experiment on fully relaxed SiGe layers will shed light on the formation mechanism of these surface islands. Such experiments are therefore planned to be performed during the following reporting period of the MUNDFAB project.

5.4. Effect of the Boron redistribution on electrical properties

In the case of B-doped samples, in addition to the Ge and B concentration profiles displayed on the Figure 12 for the reference samples (un-annealed), similar measurements have been performed by means of SIMS on laser annealed samples at Ł-IMiF. As in the undoped cases, above the melt threshold, the formation of a gradient of Ge towards the surface can be observed. However, in these samples, a complete redistribution of Boron, which differ from the Ge redistribution, has also been observed all along the SiGe layer. At this moment, it has been shown that as a function of the initial Boron dose, the melt regime and the relaxation state of the SiGe layer, different behaviour could be highlighted in the evolution of the Sheet resistance and Hall dose. As these electrical properties of the B-doped layers should be strongly linked to the Boron distribution in the samples, for future investigations it must be interesting to understand the correlation between the evolution of the Boron distribution as function of the annealing regime, the activation state of Boron atoms, and the electrical properties of the doped SiGe layers. Such works have already been launched and should be presented in a following report.

6. Conclusion

In this deliverable, numerous structural analyses have been carried out on laser annealed undoped and B-doped strained SiGe layers. These firsts experiments have shown that, independently of the Ge content, four annealing regimes can be evidenced as a function of the laser energy density. In the sub-melt regime (i.e for low energy densities), no changes are observed in the SiGe layer. In the surface melt, the SiGe layer started to melt, leading to (i) the formation of nano-islands at the surface, (ii) a redistribution of the Ge toward the layer surface, and (iii) the formation of strain relieving defects in the SiGe layers. When the partial melt is reached, similar observations are made. In this regime, the surface is entirely melted and a rough l/s interface is formed. In this case, the SiGe layer can be fully relaxed. When the full melt is reached, the l/s interface tends to flattened, and two cases can be differentiated. In fact, if the elastic energy stored in the SiGe layer is lower than 750 mJ/m², then the layer remains fully strained. However, if this energy is higher than 750 mJ/m², a bilayer structure is formed, which is constituted by a fully strained layer located under a 5 nm-thick fully relaxed layer. Concerning doped samples, structural observations are very similar. However, the introduction of Boron in the SiGe layer tends to decrease the degree of relaxation of the SiGe layer in surface and partial melt regimes. The formation of crystalline defects deteriorates the electrical properties of the SiGe layers, but, using higher doping level seems to circumvent this issue. Finally, for the following period of the MUNDFAB project, different new experiments, essentially based on the analysis of fully relaxed SiGe layers, have already started in order to complete our understanding of the surface structuration, the l/s interface roughness, and the correlation between structural and electrical properties.

References

[1] J. Boneberg, J. Nedelcu, H. Bender, et P. Leiderer, « Dynamics of the solidification of laser-annealed Si thin films », *Mater. Sci. Eng. A*, vol. 173, nº 1-2, p. 347-350, déc. 1993, doi: 10.1016/0921-5093(93)90242-7.

[2] C. Y. Ong, K. L. Pey, X. Li, X. C. Wang, C. M. Ng, et L. Chan, « Laser annealing induced high Ge concentration epitaxial SiGe layer in $Si_{1-x}Ge_x$ virtual substrate », *Appl. Phys. Lett.*, vol. 93, nº 4, p. 041112, juill. 2008, doi: 10.1063/1.2962991.

[3] D. P. Brunco, M. O. Thompson, D. E. Hoglund, M. J. Aziz, et H. -J. Gossmann, « Germanium partitioning in silicon during rapid solidification », *J. Appl. Phys.*, vol. 78, nº 3, p. 1575-1582, août 1995, doi: 10.1063/1.360251.

[4] J. F. Young, J. E. Sipe, et H. M. van Driel, « Laser-induced periodic surface structure. III. Fluence regimes, the role of feedback, and details of the induced topography in germanium », *Phys. Rev. B*, vol. 30, nº 4, p. 2001-2015, août 1984, doi: 10.1103/PhysRevB.30.2001.

[5] G. E. Jellison, D. H. Lowndes, D. N. Mashburn, et R. F. Wood, « Time-resolved reflectivity measurements on silicon and germanium using a pulsed excimer KrF laser heating beam », *Phys. Rev. B*, vol. 34, nº 4, p. 2407-2415, août 1986, doi: 10.1103/PhysRevB.34.2407.

[6] M. Weizman, N. H. Nickel, I. Sieber, et B. Yan, « Laser-induced self-organization in silicon-germanium thin films », *J. Appl. Phys.*, vol. 103, nº 9, p. 093536, mai 2008, doi: 10.1063/1.2919772.

[7] J. M. Hartmann, A. Abbadie, et S. Favier, « Critical thickness for plastic relaxation of SiGe on Si(001) revisited », *J. Appl. Phys.*, vol. 110, nº 8, p. 083529, oct. 2011, doi: 10.1063/1.3656989.

[8] D. C. Paine, D. J. Howard, N. G. Stoffel, et J. A. Horton, « The growth of strained $Si_{1-x}Ge_x$ alloys on ⟨001⟩ silicon using solid phase epitaxy », *J. Mater. Res.*, vol. 5, nº 5, p. 1023-1031, mai 1990, doi: 10.1557/JMR.1990.1023.

[9] F. Cristiano, A. Nejim, Y. Suprun-Belevich, A. Claverie, et P. L. F. Hemment, « Formation of extended defects and strain relaxation in ion beam synthesised SiGe alloys », *Nucl. Instrum. Methods Phys. Res. Sect. B Beam Interact. Mater. At.*, vol. 147, nº 1-4, p. 35-42, janv. 1999, doi: 10.1016/S0168-583X(98)00589-8.

[10] S. C. Jain et W. Hayes, « Structure, properties and applications of Ge_xSi_{1-x} strained layers and superlattices », *Semicond. Sci. Technol.*, vol. 6, nº 7, p. 547-576, juill. 1991, doi: 10.1088/0268-1242/6/7/001.

[11] C. Y. Ong *et al.*, « A low-cost method of forming epitaxy SiGe on Si substrate by laser annealing », *Appl. Phys. Lett.*, vol. 94, nº 8, p. 082104, févr. 2009, doi: 10.1063/1.3086881.

[12] G. Rengo *et al.*, « *(Invited)* Highly Doped $Si_{1-X}Ge_x$ Epitaxy in View of S/D Applications », *ECS Trans.*, vol. 98, nº 5, p. 27-36, sept. 2020, doi: 10.1149/09805.0027ecst.

[13] P. M. Mooney, « Strain relaxation and dislocations in SiGe/Si structures », *Mater. Sci. Eng. R Rep.*, vol. 17, nº 3, p. 105-146, nov. 1996, doi: 10.1016/S0927-796X(96)00192-1.